

Elastic Properties of Co/Cu Nanocomposite Nanowires

J. C. Jiménez-Sáez, A. M. C. Pérez-Martín
and J. J. Jiménez-Rodríguez

Abstract The mechanical deformation of Co/Cu composite nanowires was simulated by molecular dynamics in a state of uniaxial tensile and compressive stress. The Young's modulus and initial yield stress have been derived from the stress–strain curves at different conditions. For tensile strength, the effect of strain rate, volume/surface area ratio, temperature, and thickness ratio between Co and Cu sublayers was analyzed depending on the crystallographic orientations of the nanowires. At high values, the elastic modulus and yield stress depend on the strain rate; and some differences with the crystallographic orientation due to nonlinear effects appear. Both magnitudes diverge from the bulk values with decreasing the volume/surface area ratio, increasing in the case of $\langle 110 \rangle$ nanowires and decreasing for the other two directions. For $\langle 100 \rangle$ nanowires, grains undergo a crystallographic reorientation towards $\langle 111 \rangle$ and $\langle 110 \rangle$ directions. Besides, for these nanowires hexagonal close-packed atoms are preferably in the Co sublayer; and face-centered cubic atoms, in the Cu sublayer unlike nanowires in the other two directions. Plastic deformation takes place more easily in Cu sublayers. Nanowires show differences in the slip mechanism for $\langle 110 \rangle$ and $\langle 100 \rangle$ directions. In compression, the former system slips via both $\{111\}\langle 112 \rangle$ and $\{111\}\langle 110 \rangle$ dislocations; and the latter, only through $\{111\}\langle 112 \rangle$ dislocations.

J. C. Jiménez-Sáez (✉)

Dpto. de Física y Química Aplicadas a la Técnica Aeronáutica, E.U.I.T. Aeronáutica,
Universidad Politécnica de Madrid (UPM), 28040 Madrid, Spain
e-mail: jc.jimenez@upm.es

A. M. C. Pérez-Martín · J. J. Jiménez-Rodríguez

Dpto. de Física Aplicada III (Electricidad y Electrónica), Facultad de Ciencias Físicas,
Universidad Complutense de Madrid (UCM), 28040 Madrid, Spain
e-mail: cperez@fis.ucm.es

J. J. Jiménez-Rodríguez

e-mail: josejrr@fis.ucm.es

1 Introduction

The fabrication of nanocomposite nanowires has recently received much attention because of the interesting magnetic, superconducting and magnetotransport properties and their application in the development of high-density magnetic recording media and novel magnetic sensors [1, 2]. These studies were triggered by the discovery of giant magnetoresistance (GMR) effects [3] in certain metallic multilayers in which the interlayer exchange coupling results in antiferromagnetic alignment of the adjacent magnetic layers [4]. Specifically, NiCo [5], Co/Cu, NiFe/Cu or CoNiCu/Cu [6, 7] nanowires show anisotropic magnetoresistance (AMR) or current perpendicular to the planes giant magnetoresistance (CPP-GMR). This type of nanowires can be grown at low cost by electrodeposition from aqueous solution into nanochannel templates [8].

While designing such nanoscale devices, it is necessary to know their structural and thermo-mechanical properties since the mechanical strength of nanowires plays an important role in maintaining the structural integrity of the devices. For feature sizes of several atomic layers, surface stress may induce a large intrinsic compressive stress in the interior of nanowires, and their structure becomes unstable. Thus, under some conditions, the nanowires may transform from one orientation to another spontaneously [9] or, even initiate phase transformations [10]. Molecular dynamics (MD) simulations have been performed extensively and reported in published literature for composite nanowire property characterizations including phase transformation behavior at nanoscale, mechanisms of dislocation formation, plastic region and breaking under stress.

In this work, the stress–strain relations of Co/Cu multilayered nanowires under extension and compression and different conditions by means of MD simulations are obtained. The elastic modulus and initial yield stress are mainly analyzed. The knowledge of these mechanical properties will be helpful to the design, manufacture and manipulation of nanodevices. Effects of composition, size, strain rate and temperature on the extension properties are discussed in detail as a function of the crystallographic orientation. Influence of internal structure and interface on the mechanical behavior of nanostructures is discussed. The nanostructural deformation for tensile and compressive stresses is presented together with an identification of dislocations.

2 Computational Method

The interaction among atoms is essentially determined by the atomic potential. In our case, the used potential for the Co–Cu system was elaborated by Levanov et al. [11] in the second-moment tight-binding approximation (TB-SMA) [12]. This potential fits experimentally lattice constants, cohesive energies and elastic

constants for Cu (face-centered cubic, fcc) and Co (hexagonal close-packed, hcp) and takes into account ab initio properties of small Co clusters on Cu surfaces. In this model, the cohesive energy E_i of an atom i is:

$$E_i = \sum_{j(\neq i)} \frac{1}{2} V^{\alpha\beta}(r_{ij}) + F(\rho_i) = \sum_{j(\neq i)} \frac{1}{2} V^{\alpha\beta}(r_{ij}) - (\rho_i)^{1/2} \quad (1)$$

$$\rho_i = \sum_{j(\neq i)} \Phi^{\alpha\beta}(r_{ij})$$

where α and β refer to the chemical nature of the atoms i and j , respectively; and r_{ij} is the distance between them. The first term, repulsive term, is described by a pairwise potential energy of the modified Born-Mayer type. The second term, attractive term, contains the many-body interaction that models the band energy.

From this magnitude, the stress tensor σ^{kl} can be obtained as the derivative of the total energy per unit volume [13]. Using a TB-SMA potential, this tensor can be expressed as:

$$\sigma^{kl} = \frac{1}{V} \sum_i \frac{\partial E_i}{\partial \varepsilon^{kl}} = \frac{1}{V} \sum_i \left(-m_i v_i^k v_i^l + \frac{1}{2} \sum_{j(\neq i)} (h_{ij}) \frac{r_{ij}^k r_{ij}^l}{r_{ij}} \right) \quad (2)$$

$$h_{ij} = \frac{\partial V^{\alpha\beta}}{\partial r_{ij}}(r_{ij}) + \left(\frac{\partial F}{\partial \rho_i}(\rho_i) + \frac{\partial F}{\partial \rho_j}(\rho_j) \right) \frac{\partial \Phi^{\alpha\beta}}{\partial r_{ij}}(r_{ij})$$

where ε^{kl} is the strain-tensor Cartesian component kl ($k, l \in x, y, z$), v^k is the speed component k , and V the system volume. Each element of the summation divided by the effective atomic volume is the local stress at the atom site i . The main part of this work is carried out on a so-called reference nanowire. This system is a set of seven epitaxial ultrathin layers composed of two fcc oriented Co and Cu sublayers of about 10 nm thick each one stacked up alternately to build a Co/Cu multilayered nanowire. For this thickness, Co/Cu nanowires exhibit a large giant magnetoresistance (GMR) of 20–30% [14]. The presence of Co/Cu interfaces and the lattice mismatch favors an fcc phase for Co [14]. A circular cross-sectional shape of 5.11 nm in diameter has been considered. This size was selected since it can be built and investigated experimentally [15], and even though the simulation time is long, it is still reasonable. The thickness ratio between Co and Cu sublayers and the transverse and longitudinal dimensions have been varied.

Prior to uniaxial loading, the nanowires were relaxed and thermally equilibrated at 300 K using a Nosé–Hoover thermostat [16] while keeping periodic boundary conditions in the main nanowire direction. Then, boundary conditions were removed and the system was again relaxed at that temperature by using a constant pressure algorithm for 30 ps [17]. This procedure causes the pre-stress to be set to zero in the lattice. Finally, the uniaxial tensile and compressive loading process of nanowires was simulated at the temperature of 300 K and a strain rate of 10^9 s^{-1} . Nevertheless, other strain rates and temperatures have also been considered in the

present work. The Nosé–Hoover thermostat gives rise to modest temperature fluctuations, which leads to correct canonical averages of system properties. The uniaxial loading is reached by applying velocity to the atoms of both ends. This velocity varies linearly from zero to the maximum value, thus creating a ramp velocity profile. Such a ramp velocity is used to avoid the emission of shock waves.

To provide information on the atomic displacement in dislocations, we calculate the slip vector [18] and the maximum magnitude of slip vector, defined respectively for an atom i as:

$$\vec{s}_i = -\frac{1}{n_s} \sum_{j(\neq i)}^n (\vec{r}_{ij} - \vec{R}_{ij}) ; \quad s_{i,\max} = \max_{j=1,\dots,n_s} |\vec{r}_{ij} - \vec{R}_{ij}| \quad (3)$$

where r_{ij} and R_{ij} are the vector differences of atoms i and j at the current and reference positions, respectively; n is the number of nearest neighbors to atom i ; and n_s is the number of slipped neighbors. The reference positions are associated with the state of zero mechanical stress. The slip vector coincides with the Burgers vector for the slip of adjacent atomic planes, where the atom lies on one of those planes. For any other inhomogeneous deformation, the slip vector will provide quantitative information about the deformation. The maximum magnitude of slip vector has also been calculated to assess the margin of error in predictions. The internal relocation of atoms has been studied by the common-neighbor analysis (CNA) [19] and the lattice unit vectors (crystallographic orientation) in each grain [20].

3 Results and Discussion

In a similar way to that for pure metals [21], the stress curve as a function of the engineering strain for a Co/Cu composite nanowire in tensile loading at normal and low strain rates ($<5 \cdot 10^9 \text{ s}^{-1}$) increases up to an absolute maximum in the elastic region. In Fig. 1, stress–strain curves at different strain rates and orientation are shown. The $\langle 100 \rangle$ orientation exhibits a very linear stress–strain relationship [22]. The initial yield stress (or strain) is defined as the stress (or strain) at the elastic limit that, for these values of strain rate, coincides with the absolute maximum. After reaching the peak value, the stress goes down dramatically due to the occurrence of dislocations. Then, the plastic zone is developed. In this region, the curve is saw-shaped, and at high strain rates it softly decreases. Plasticity comes from the emission and movement of different dislocation systems. The elastic zone can end in a relative maximum at rates of the order of $5 \cdot 10^{10} \text{ s}^{-1}$, especially for $\langle 110 \rangle$ and $\langle 100 \rangle$ directions. Then, a strain hardening region is developed and it is necessary to distinguish between yield and ultimate (absolute maximum) stresses.

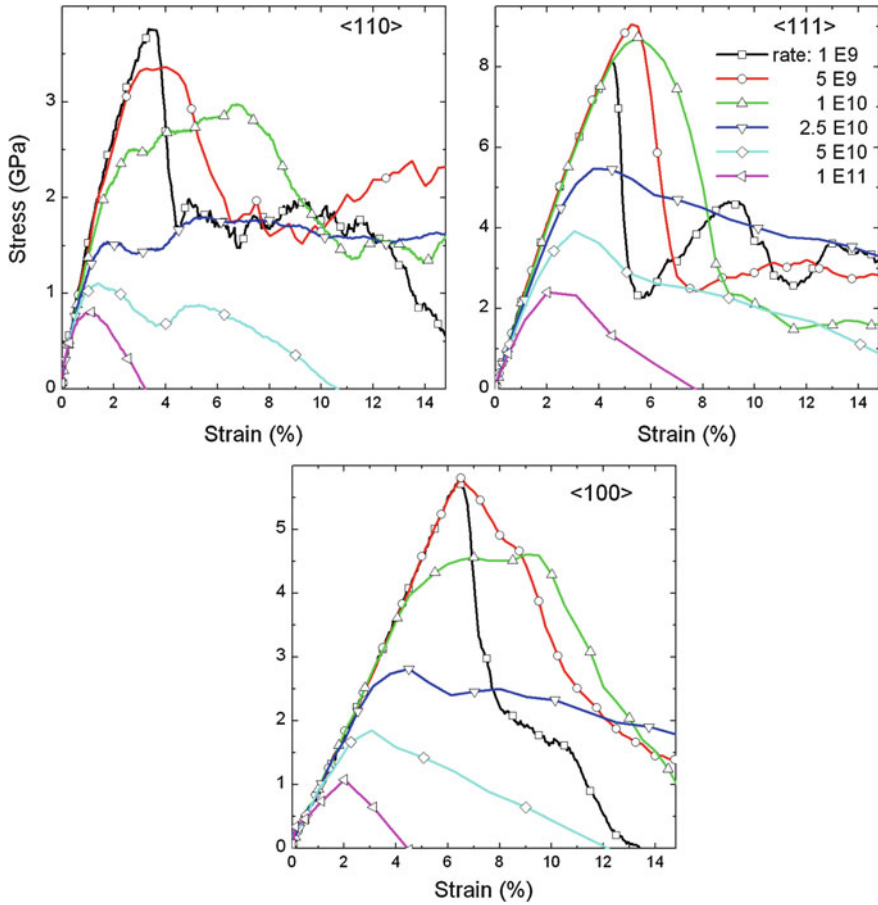
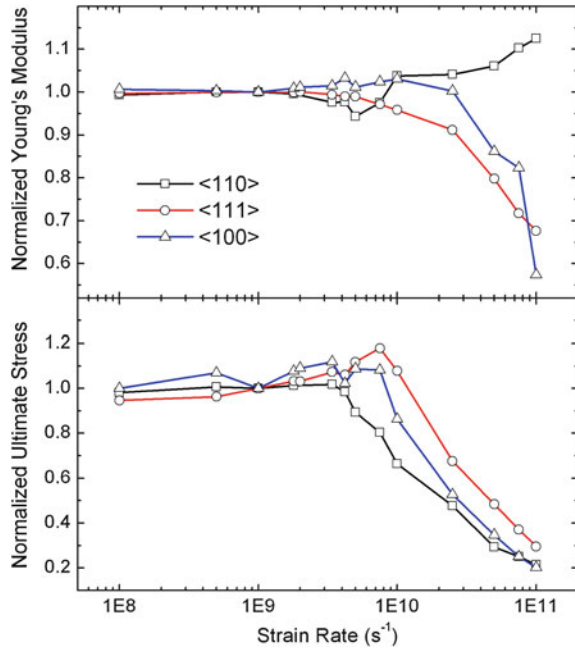


Fig. 1 Stress–strain curves for a reference nanowire at different strain rate and crystallographic orientations and 300 K

The stress curve is linear only at low strain in the elastic region. Wu [22] indicated that the nonlinearity may come from the inhomogeneity of nanowire cross-section, especially important in multilayers due to the lattice mismatch. The Young’s or elastic modulus is determined from the slope by applying a linear fit at low strain. The stress required for homogeneous dislocation nucleation is highly dependent on the crystallographic orientation and the uniaxial loading conditions [23]; thus, certain orientations require a higher stress in tension, e.g., $\langle 111 \rangle$ nanowires. Besides, these nanowires are the hardest one (larger elastic modulus). In Fig. 2, the Young’s modulus (rough, in some cases) and ultimate stress as a function of the strain rate are indicated. 146, 209, 76 GPa are the elastic moduli; and 3.76, 8.10, 5.74 GPa, the yield stresses used for the normalization in $\langle 110 \rangle$, $\langle 111 \rangle$ and $\langle 100 \rangle$ directions, respectively. The elastic modulus and yield stress are

Fig. 2 Normalized Young's modulus and ultimate stress as a function of the strain rate for the reference nanowire with different crystallographic orientations and 300 K

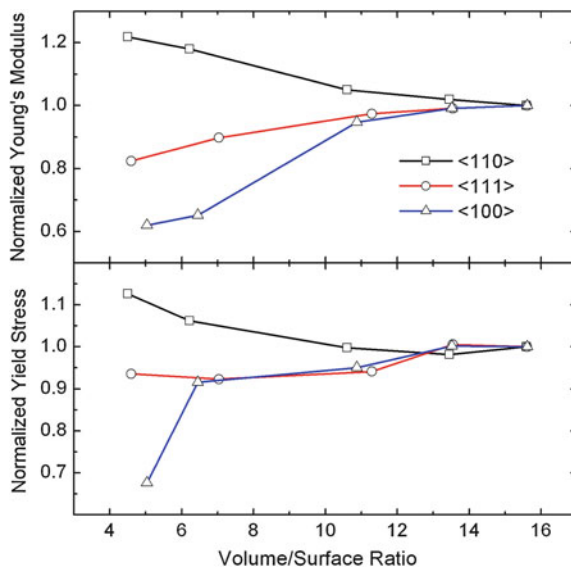


approximately independent of strain rate, except at high strain rates ($>5 \cdot 10^9 \text{ s}^{-1}$). The effect of strain rate on the mechanical behavior is similar for the three crystallographic orientations, except for $\langle 110 \rangle$ nanowires. In this case, the increase in elastic modulus with increasing strain rate is due to the nonlinearity of the stress curve. If the nanowire diameter decreases, this distinguishing behavior does not exist.

Size effects on the elastic behavior have also been analyzed. A parameter as the volume-to-surface-area (vol/sa) ratio (normalized by the vol/sa ratio of the Cu unit cell) is introduced. The dependence of Young's modulus and initial yield stress on this parameter is represented in Fig. 3 for the tensile regime. The smallest nanowire had 1.50 nm maximum wide (5-Co/Cu-layer long), and the largest one, 5.11 nm (reference nanowire). Below a ratio of about 10, both mechanical magnitudes diverge from the bulk value, increasing in the case of $\langle 110 \rangle$ orientation and decreasing for the other two directions. This behavior is in accordance with previous works on pure Cu, Ag and Au nanowires [24–26]. The surface effect plays an important role on the mechanical properties, since, in fact, the different 'core-shell' elasticity [27] and the nonlinear elastic response of the nanowire core induced by the surface stress [24] are determining factors of the elastic modulus.

Two details deserve to be mentioned in the break-up layer of a nanowire of 2.24 nm in diameter (ratio about 6.5): For $\langle 100 \rangle$ nanowires, grains undergo a crystallographic reorientation, thus it is possible to find mainly $\langle 111 \rangle$ -oriented and also $\langle 110 \rangle$ -oriented grains. A similar reorientation process towards $\langle 110 \rangle$ direction

Fig. 3 Normalized Young's modulus and initial yield stress as a function of the normalized vol/sa ratio for nanowires with different crystallographic orientations (at 300 K and 10^9 s^{-1})



is observed in an fcc gold $\langle 100 \rangle$ nanowire [28]. Besides, after the break-up the number of hcp atoms is larger for $\langle 100 \rangle$ nanowires (2.5 times) than the number of fcc atoms unlike $\langle 111 \rangle$ and $\langle 110 \rangle$ directions (the former has 3.2 times more fcc than hcp atoms, and the later 4.5). These hcp atoms are preferably in the Co sublayer for $\langle 100 \rangle$ direction (there are two times more hcp Co than Cu atoms), and in the Cu sublayer for $\langle 111 \rangle$ (two times more hcp Cu than Co atoms) and $\langle 110 \rangle$ (there are only hcp Cu atoms) directions. The fcc atoms are preferably in the Cu sublayer for $\langle 100 \rangle$ nanowires (two times more fcc Cu than Co atoms) and in the Co sublayer for $\langle 111 \rangle$ and $\langle 110 \rangle$ nanowires (two times more fcc Co than Cu atoms in both cases). Therefore, in the break-up zone Co recovers an hcp structure more easily for $\langle 100 \rangle$ nanowires, and in addition Cu is more stable in its fcc structure for $\langle 111 \rangle$ and $\langle 110 \rangle$ nanowires.

In Fig. 4, the Young's modulus and initial yield stress at different temperatures for the reference nanowire are represented. Both magnitudes decrease approximately linearly with increasing temperature [29]. The deviation from the horizontal line is larger in the case of $\langle 100 \rangle$ direction, and therefore, temperature has more influence on the mechanical behavior of this orientation. The drop of the elastic modulus with increasing temperature is associated with the significantly weakened bond forces due to the larger thermal vibrations of atoms [30]. Nevertheless, temperature has no substantial effect on the deformation mechanism [30]. The dislocation nucleation takes place more easily at higher temperatures. Theoretical models of dislocation emission from a crack tip show a definitive relationship between activation energy and temperature [31]. This effect leads to decrease the yield stress. Absolute values of yield stress in these three directions at different temperature are slightly smaller than other published values on pure Cu nanowires due probably to the different simulation potential [32].

Fig. 4 Normalized Young's modulus and initial yield stress as a function of temperature for the reference nanowire with different crystallographic orientations at 10^9 s^{-1}

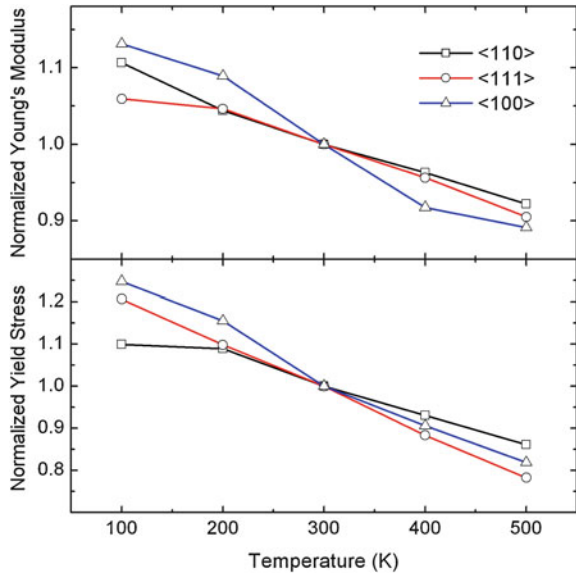
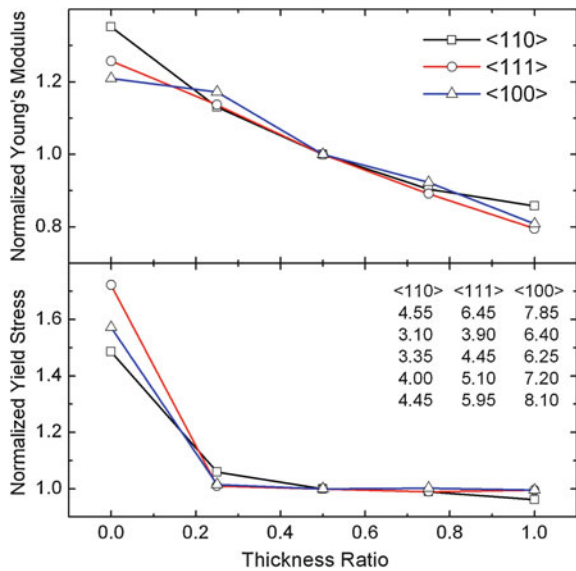
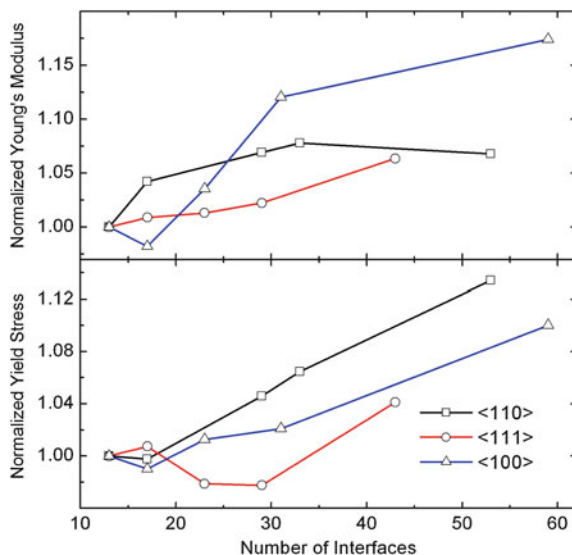


Fig. 5 Normalized Young's modulus and initial yield stress as a function of the thickness ratio between Co and Cu sublayers for the reference nanowire with different crystallographic orientation (at 300 K and 10^9 s^{-1}). For pure Co, thickness ratio is 0; and for Cu, 1. Corresponding values of the yield strain (%) are indicated numerically from small to large thickness



The elastic modulus of Co/Cu nanowires decreases with increasing thickness of Cu sublayer in a similar way to that obtained in other bimetallic multilayers [33]. In fact, both magnitudes are much larger for Co nanowires than for Cu nanowires. In Fig. 5, the Young's modulus and yield stress are represented as a function of the thickness ratio between Co and Cu sublayers. While the Young's modulus decreases gradually, yield stress falls steeply from pure Co value to the pure Cu

Fig. 6 Normalized Young's modulus and initial yield stress as a function of the number of interfaces for nanowires with different crystallographic orientations and the same length (at 300 K and 10^9 s^{-1})



value for any Cu sublayer thickness. In fact, lattice distortion takes place firstly and fundamentally in Cu sublayers, even for small thicknesses of these [33]. A reason is that for this potential the stacking-fault energy of Cu is 19 mJm^{-2} , and of Co is 25 mJm^{-2} .

The lattice misfit at the interface may also have influence on the mechanical properties. Cu has a lattice parameter of 3.615 \AA and fcc Co of 3.544 \AA . Therefore, Cu sublayers should experience an additional tensile stress, and Co sublayers should experience a compressive stress (Poisson effect). Figure 6 shows the normalized Young's modulus and yield stress as a function of the number of interfaces for a Co/Cu nanowire with the same length. The elastic modulus and yield stress increase with increasing number of interfaces, especially for $\langle 100 \rangle$ and $\langle 110 \rangle$ directions. Diameter of these nanowires is 3.5 times lower than that necessary to create a misfit dislocation. Therefore, in this case internal stresses influence only moderately the mechanical properties. Additional studies on this subject are necessary, especially for different diameters and/or large misfit [33, 34].

The magnitude of Burgers vector of a $\{111\}\langle 112 \rangle$ partial dislocation in Cu is 1.48 \AA , and of a $\{111\}\langle 110 \rangle$ full dislocation is 2.56 \AA . Therefore, from the distribution of magnitude of slip vector, it is possible to know the existence of stacking faults and full dislocations. The components of slip vector allow to know the specific partial dislocation nucleated on a $\{111\}$ plane. In Fig. 7, an image of three nanowires in tension and their corresponding distributions of magnitude and maximum magnitude of slip vector are shown. Yielding of nanowires occurs through the nucleation from edges and propagation across the nanowires of $\{111\}\langle 112 \rangle$ partial dislocations (see in Fig. 7 the top nanowire). Dislocation nucleation in a nanowire seems to be related to the effective critical resolved shear stress (RSS) caused by the external forces in the leading slip direction on the slip plane [37]. According to the

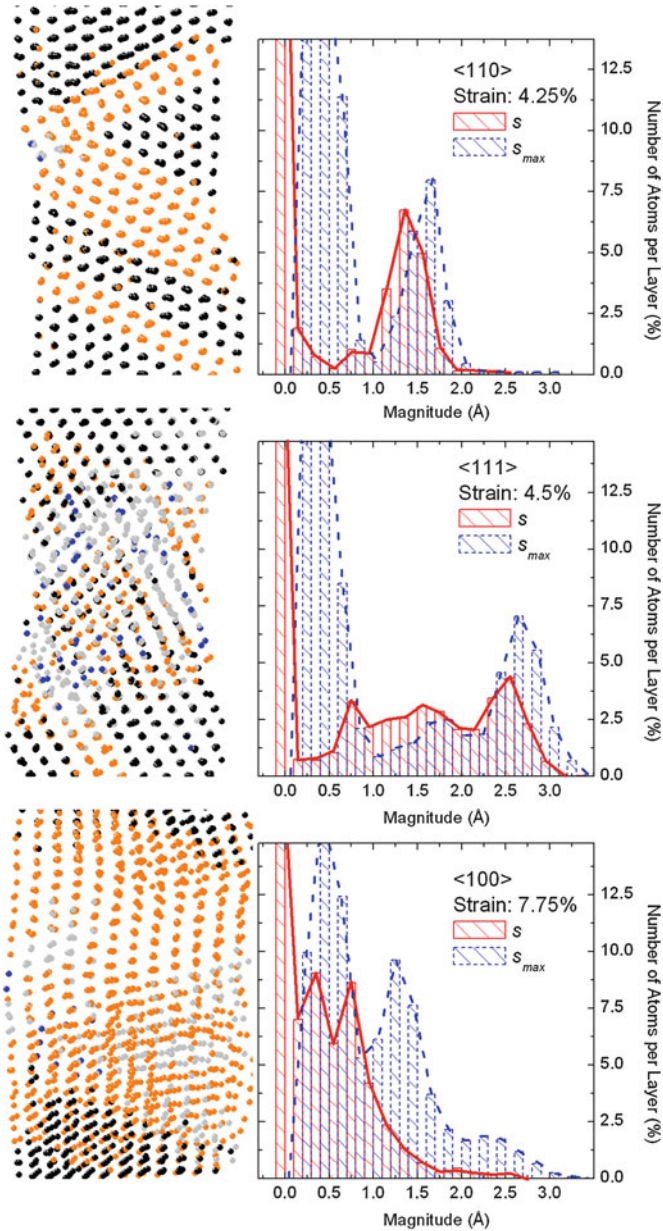
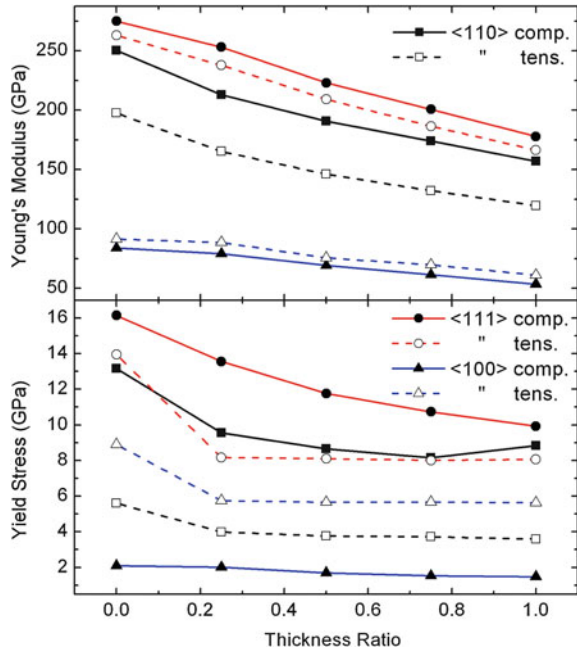


Fig. 7 Projection of three nanowires of 2.24 nm in diameter (at 300 K and 10^9 s^{-1}). The vertical axis (nanowire axis) corresponds to $\langle 110 \rangle$, $\langle 111 \rangle$ and $\langle 100 \rangle$ directions (from *top* to *bottom*), and the horizontal one, to $\langle 00-1 \rangle$, $\langle 11-2 \rangle$ and $\langle 001 \rangle$ directions, respectively. Colors are assigned according to the values of $s_{i,max}$: *black* ($s_{i,max} < 0.7$), *grey* (*orange*) ($0.7 < s_{i,max} < 2$), *light grey* ($2 < s_{i,max} < 3$) and *light black* (*blue*) ($s_{i,max} > 3$). Beside this representation, the distributions of magnitude s and maximum magnitude s_{max} of slip vector are shown

Fig. 8 Young's modulus and initial yield stress as a function of the thickness ratio between Co and Cu sublayers for the reference nanowire with different crystallographic orientation and tensile and compressive stresses (at 300 K and 10^9 s^{-1})



distributions of magnitude and maximum magnitude of slip vector in Fig. 7, $\langle 110 \rangle$ nanowires slip via $\{111\}\langle 112 \rangle$ partial dislocation nucleation and propagation. Unlike, in $\langle 111 \rangle$ nanowires, both $\{111\}\langle 112 \rangle$ and $\{111\}\langle 110 \rangle$ slips occur, the latter occurs through two successive $\{111\}\langle 112 \rangle$ slips on the same $\{111\}$ plane. Finally, in $\langle 100 \rangle$ nanowires, the magnitude of slip vector is not always an indicative factor of the type of generated dislocations since other defects mask slips, given the small space in which the yielding process takes place [35]. Due to this, the maximum magnitude of slip vector is used. In this case, both $\{111\}\langle 112 \rangle$ and $\{111\}\langle 110 \rangle$ slips occur, although the frequency of appearance of the first type is larger. Au $\langle 100 \rangle$ nanowires show the same behavior, however Au $\langle 111 \rangle$ nanowires, in tensile yielding, only nucleate $\{111\}\langle 112 \rangle$ partial dislocations [36].

Other interesting aspect is that the Young's modulus and yield stress are larger in compression than in tension, except for $\langle 100 \rangle$ direction. This asymmetry may be primarily due to effects of surface stresses and the different slip systems active during tensile and compressive yielding [37]. In Fig. 8 both magnitudes are represented as a function of the thickness ratio. The uniaxial Schmidt factor for leading partial slip is larger under compression than under tension for $\langle 100 \rangle$ nanowires unlike for the other two directions; and thus, for these nanowires, it is easier to yield under compression [26, 37]. Differences between tension and compression for both magnitudes are larger for $\langle 110 \rangle$ direction, especially in the case of the elastic modulus. Besides, differences for this magnitude are independent of the thickness ratio. Unlike, the gap for the yield stress between both loading processes is larger in general whether the nanowire is made only of Co.

According to the distributions obtained from the vector slip, nanowires show differences in the slip mechanism for $\langle 110 \rangle$ and $\langle 100 \rangle$ directions (not for $\langle 111 \rangle$ direction). In compression, the former system slip via both $\{111\}\langle 112 \rangle$ and $\{111\}\langle 110 \rangle$ dislocations, and the latter only through $\{111\}\langle 112 \rangle$ dislocations. It is well known that for bulk single crystal the plastic deformation mode depends on the relationship between the Schmidt factor of the leading partial dislocation and that of the trailing partial dislocation. Full dislocation slipping prefers to be activated if the Schmidt factor of the trailing partial dislocation is larger than that of the leading partial dislocation [26, 38]. In our case, the only case in that this rule is not verified is for the $\langle 111 \rangle$ direction in tension in a similar way to what happens in other systems like Au [26].

4 Summary and Conclusions

The mechanical deformation properties of Co/Cu multilayered nanowires (5 nm in diameter \times 140 nm long) have been studied by MD under uniaxial tensile and compressive stresses at different crystallographic orientations ($\langle 110 \rangle$, $\langle 111 \rangle$, $\langle 100 \rangle$). The elastic modulus and initial yield stress are approximately independent of strain rate, except at high strain rates. The effect of strain rate on the mechanical behavior is similar for the three crystallographic orientations, except the increase in elastic modulus with increasing strain rate for $\langle 110 \rangle$ nanowires due to the nonlinearity of the stress curve.

Below a normalized vol/sa ratio of about 10, elastic modulus and initial yield stress for tensile strength diverge from the bulk value, increasing in the case of $\langle 110 \rangle$ orientation and decreasing for the other two directions. In the break-up Co/Cu layer for $\langle 100 \rangle$ nanowires, grains undergo a crystallographic reorientation towards $\langle 111 \rangle$ and $\langle 110 \rangle$ directions. Besides, in this layer after the break-up the number of hcp atoms is larger than the number of fcc atoms only for $\langle 100 \rangle$ nanowires. These hcp atoms are preferably in the Co sublayer unlike the other two directions. The fcc atoms are preferably in the Cu sublayer for $\langle 100 \rangle$ nanowires unlike the other two directions. Young's modulus and yield stress decrease approximately linearly with increasing temperature. Temperature has more influence on the mechanical behavior of $\langle 100 \rangle$ orientation.

$\langle 110 \rangle$ nanowires slip via $\{111\}\langle 112 \rangle$ partial dislocation nucleation and propagation. Unlike, in $\langle 111 \rangle$ nanowires, both $\{111\}\langle 112 \rangle$ and $\{111\}\langle 110 \rangle$ slips occur, the latter occurs through two successive $\{111\}\langle 112 \rangle$ slips on the same $\{111\}$ plane. In $\langle 100 \rangle$ nanowires, both $\{111\}\langle 112 \rangle$ and $\{111\}\langle 110 \rangle$ slips occur, although the frequency of appearance of the first type is larger. Young's modulus and yield stress are larger in compression than in tension, except for $\langle 100 \rangle$ direction. The uniaxial Schmidt factor for leading partial slip, in addition to effects of surface stresses and the different active slip systems explain this circumstance. Differences between tension and compression for both magnitudes are larger for $\langle 110 \rangle$ direction, and in the case of elastic modulus they are independent of the thickness

ratio. Tension and compression show differences in the slip mechanism for $\langle 110 \rangle$ and $\langle 100 \rangle$ directions. In compression, the former system slips via both $\{111\}\langle 112 \rangle$ and $\{111\}\langle 110 \rangle$ dislocations; and the latter, only through $\{111\}\langle 112 \rangle$ dislocations. The relationship between the Schmidt factor of the leading and the trailing partial dislocations can explain this effect for these two directions, but not for $\langle 111 \rangle$ direction that does not show differences in the slip mechanisms.

Acknowledgments This work was supported by the Universidad Complutense of Madrid under the Project for Research Groups (Bioelectromagnetism Research Group 910305-4120909).

References

1. Whitney, T.M., Searson, P.C., Jiang, J.S., Chien, C.L.: Fabrication and magnetic properties of arrays of metallic nanowires. *Science* **261**, 1316 (1993)
2. Wernsdorfer, W., Doudin, B., Mailly, D., Hasselbach, K., Benoit, A., Meier, J., Ansermet, J-Ph, Barbara, B.: Nucleation of magnetization reversal in individual nanosized nickel wires. *Phys. Rev. Lett.* **77**, 1873 (1996)
3. Baibich, M.N., Broto, J.M., Fert, A.: Nguyen Van Dau, F., Petroff, F., Etienne, P., Creuzet, G., Friederich, A., Chazelas, J.: Giant magnetoresistance of $(001)\text{Fe}/(001)\text{Cr}$ magnetic superlattices. *Phys. Rev. Lett.* **61**, 2472 (1988)
4. Parkin, S.S.P., Bhadra, R., Roche, K.P.: Oscillatory magnetic exchange coupling through thin copper layers. *Phys. Rev. Lett.* **66**, 2152 (1991)
5. Wegrowe, J.E., Gilbert, S.E., Kelly, D., Doudin, B., Ansermet, J-Ph: Anisotropic magnetoresistance as a probe of magnetization reversal in individual nano-sized nickel wires. *IEEE Trans. Magn.* **34**, 903 (1998)
6. Piraux, L., George, J.M., Despres, J.F., Leroy, C., Ferain, E., Legras, R., Ounadjela, K., Fert, A.: Giant magnetoresistance in magnetic multilayered nanowires. *Appl. Phys. Lett.* **65**, 2484 (1994)
7. Blondel, A., Meier, J.P., Doudin, B., Ansermet, J-Ph: Giant magnetoresistance of multilayers in nanowires. *Appl. Phys. Lett.* **65**, 3019 (1994)
8. Martin, C.R.: Nanomaterials: A membrane-based synthetic approach. *Science* **266**, 1961 (1994)
9. Liang, W.W., Zhou, M.: Pseudoelasticity of single crystalline Cu nanowires through reversible lattice reorientations. *J. Eng. Mater. Technol.* **127**, 423 (2005)
10. Diao, J., Gall, K., Dunn, M.L.: Atomistic simulation of the structure and elastic properties of gold nanowires. *J. Mech. Phys. Solids* **52**, 1935 (2004a)
11. Levanov, N.A., Stepanyuk, V.S., Hergert, W., Bazhanov, D.I., Dederichs, P.H., Katsnelson, A.A., Massobrio, C.: Energetics of Co adatoms on the Cu(001) surface. *Phys. Rev. B* **61**, 2230 (2000)
12. Cleri, F., Rosato, V.: Tight-binding potentials for transition metals and alloys. *Phys. Rev. B* **48**, 22 (1993)
13. Zubarev, D.N.: *Non-Equilibrium Statistical Thermodynamics*. Nauka, Moscow (1971)
14. Scarani, V., Doudin, B., Ansermet, J.P.: The microstructure of electrodeposited cobalt-based nanowires and its effect on their magnetic and transport properties. *J. Magn. Magn. Mater.* **205**, 241 (1999)
15. Routkevich, D., Tager, A.A., Haruyama, J., Almalawi, D., Moskovits, M., Xu, J.M.: Non-lithographic nanowire arrays: Fabrication, physics and device applications. *IEEE Trans. Electron Devices* **43**, 1646 (1996)
16. Hoover, W.R.: Canonical dynamics: Equilibrium phase-space distributions. *Phys. Rev. A* **31**, 1695 (1985)
17. Parrinello, M., Rahman, A.: Polymorphic transitions in single crystals: A new molecular dynamics method. *J. Appl. Phys.* **52**, 7182 (1981)

18. Zimmerman, J.A., Kelchner, C.L., Klein, P.A., Hamilton, J.C., Foiles, S.M.: Surface step effects on nanoindentation. *Phys. Rev. Lett.* **87**, 165507 (2001)
19. Cleveland, C.L., Luedtke, W.D., Landman, U.: Melting of gold clusters. *Phys. Rev. B* **60**, 5065 (1999)
20. Jiménez-Sáez, J.C., Pérez-Martín, A.M.C., Jiménez-Rodríguez, J.J.: Structural changes in metallic nanoclusters deposited on substrates with much larger lattice parameters. In: Dirote, E.V. (ed.) *New Developments in Nanotechnology Research*. Nova Science Publishers, New York (2006)
21. Wu, H.A.: Molecular dynamics study of the mechanics of metal nanowires at finite temperature. *Euro J. Mech. A Solids* **25**, 370 (2006a)
22. Wu, H.A.: Molecular dynamics study on mechanics of metal nanowire. *Mech. Res. Commun.* **33**, 9 (2006b)
23. Tschopp, M.A., McDowell, D.L.: Tension-compression asymmetry in homogeneous dislocation nucleation in single crystal copper. *Appl. Phys. Lett.* **90**, 121916 (2007)
24. Liang, H., Upmanyu, M., Huang, H.C.: Size-dependent elasticity of nanowires: Nonlinear effects. *Phys. Rev. B* **71**, 241403 (2005)
25. McDowell, M.T., Leach, A.M., Gall, K.: On the elastic modulus of metallic nanowires. *Nano Lett.* **8**, 3613 (2008)
26. Wen, Y.-H., Zhang, Y., Wang, Q., Zheng, J.-C., Zhu, Z.-Z.: Orientation-dependent mechanical properties of Au nanowires under uniaxial loading. *Comput. Mater. Sci.* **48**, 513 (2010)
27. Miller, R.E., Shenoy, V.B.: Size-dependent elastic properties of nanosized structural elements. *Nanotechnology* **11**, 139 (2000)
28. Diao, J., Gall, K., Dunn, M.L.: Surface stress driven reorientation of gold nanowires. *Phys. Rev. B* **70**, 075413 (2004b)
29. Setoodeh, A.R., Attariani, H., Khosrownejad, M.: Atomistic simulation on size-dependent yield strength and defects evolution of metal nanowires. *Comput. Mater. Sci.* **44**, 378 (2008)
30. Koh, S.J.A., Lee, H.P., Lu, C., Cheng, Q.H.: Molecular dynamics simulation of solid platinum nanowire under uniaxial tensile strain: A study on temperature and strain rate effects. *Phys. Rev. B* **72**, 085414 (2005)
31. Zhang, Y.W., Wang, T.C., Tang, Q.H.: The effect of thermal activation of crack processes at an atomistic crack tip. *J. Phys. D* **28**, 748 (1995)
32. Tschopp, M.A., Spearot, D.E., McDowell, D.L.: Atomistic simulations of homogeneous dislocation nucleation in single crystal copper. *Modelling Simul. Mater. Sci. Eng.* **15**, 693 (2007)
33. Ma, F., Song, Z.-X., Li, Y.-H., Xu, K.-W.: Plastic deformation in bi-metal multilayer nanowires. *Microelectron. Eng.* **87**, 426 (2010)
34. Jiménez-Sáez, J. C., Pérez-Martín, A. M. C., Jiménez-Rodríguez, J. J.: Mechanical characterization of Co/Cu multilayered nanowires. *J. Nanosci. Nanotechnol.*, in press (2012)
35. Hua, J., Hartmaier, A.: Determining Burgers vectors and geometrically necessary dislocation densities from atomistic data. *Modelling Simul. Mater. Sci. Eng.* **18**, 045007 (2010)
36. Diao, J., Gall, K., Dunn, M.L., Zimmerman, J.A.: Atomistic simulations of the yielding of gold nanowires. *Acta Materialia* **54**, 643 (2006)
37. Diao, J., Gall, K., Dunn, M.L.: Yield strength asymmetry in metal nanowires. *Nano Lett.* **4**, 1863 (2004c)
38. Lin, Y.C., Pen, D.J.: Analogous mechanical behaviors in $\langle 100 \rangle$ and $\langle 110 \rangle$ directions of Cu nanowires under tension and compression at a high strain rate. *Nanotechnology* **18**, 395705 (2007)